Articles

Hydrophobic Core Fluidity of Homologous Protein Domains: Relation of Side-Chain Dynamics to Core Composition and Packing[†]

Robert B. Best,* Trevor J. Rutherford, Stefan M. V. Freund, and Jane Clarke

Cambridge University Chemical Laboratory, MRC Centre for Protein Engineering, Lensfield Road, Cambridge CB2 1EW, U.K.

Received September 15, 2003; Revised Manuscript Received October 31, 2003

ABSTRACT: The side-chain dynamics of methyl groups in two structurally related proteins from the fibronectin type III (fnIII) superfamily, the third fnIII domain from human tenascin (TNfn3) and the tenth fnIII domain from human fibronectin (FNfn10), have been studied by NMR spectroscopy. Side-chain order parameters reveal that the hydrophobic cores of the two proteins have substantially different mobilities. The core of TNfn3 is very dynamic, with exceptionally low order parameters for the most deeply buried residues, while that of FNfn10 is more like those of other proteins which have been studied with this technique, having a relatively rigid core with uniformly distributed dynamics. The unusually dynamic core of TNfn3 appears to be related to its amino acid composition, which makes it more fluid-like. A further explanation for the mobility of the TNfn3 core may be found in the negative correlation between the order parameter and excess packing volume, which shows that the core of TNfn3 is less densely packed and consequently has lower methyl order parameters for its buried residues. Rotameric transitions, presumably facilitated by the lower packing density, appear to make an important contribution to lowering the order parameters, and have been probed by measuring three-bond scalar couplings. Overall, although backbone dynamics is generally similar for proteins with the same topology on a fast time scale (picoseconds to nanoseconds), this study shows that a single fold can accommodate a wide variation in the dynamic properties of its core.

The importance of the native state dynamics of proteins to their physical properties and functions has long been recognized (*1*). While many experimental methods of studying protein mobility are available, few can match the resolution of high-field NMR spectroscopy, which can yield information about motions on time scales ranging from picoseconds to seconds at the resolution of individual residues (*2*). Backbone dynamics experiments utilizing NMR relaxation data (*3*, *4*) have now been used for dozens of systems, and more recently, analogous side-chain dynamics experiments have been developed (*5*−*8*), revealing substantial mobility even for buried side chains.

Studying structurally homologous proteins makes it possible to understand the relation among the overall fold topology, local structure, and dynamics. Such comparative studies assume an added importance, given that it has been shown from the large number of protein structures determined in recent years that most protein domains can be organized into relatively few families similar in backbone structure (*9*−*11*). A number of backbone dynamics studies on homologous domains (*12*−*14*) have shown that there are usually similarities on a picosecond to nanosecond time scale for residues in secondary structure elements. Indeed, a simple heuristic equation has recently been developed which can predict backbone amide order parameters based purely on structural parameters (the number of contacts made by the amide proton and the carbonyl oxygen of the preceding residue) (*15*). There can nonetheless be significant differences in loop mobilities as well as localized differences in motion on a slower microsecond to millisecond time scale which confirm the importance of sequence-specific interactions. A few studies of side-chain methyl dynamics using deuterium relaxation have also been performed on domains with related structure, although little explicit comparison has been made. Comparison of wild type ubiquitin with a variant with a redesigned hydrophobic core revealed similar overall dynamics but a redistribution of the most mobile regions of the core (*16*), the dynamics of side chains in the binding pockets of two homologous fatty acid binding proteins was related to their binding specificity (*13*), three SH2 domains have been separately studied (*17*−*19*) and compared with respect to peptide binding, and the dynamics of the homologous N- and C-terminal domains of calmodulin have been extensively reported (*20*−*22*) without explicit comparison.

In this paper, we compare the dynamics of two members of the fibronectin type III (fnIII) superfamily, one of the most common superfamilies in the sequence database: the third fnIII domain from human tenascin (TNfn3) and the tenth

[†] R.B.B. is supported by the Cambridge Commonwealth Trust, and J.C. is a Wellcome Trust Senior Research Fellow.

* To whom correspondence should be addressed. E-mail: rbb24@cam.ac.uk.

10.1021/bi035658e CCC: $27.50
Published on Web 01/16/2004

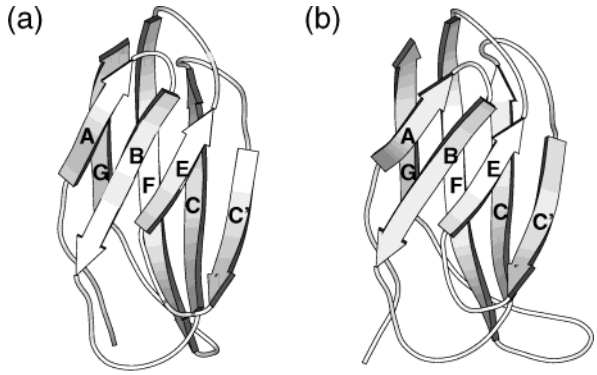

(c)

```
          1         10        20        30
TNfn3     rlDAPSQIEVkDVTdTTALITWfkPLAeId
FNfn10    vsDVPRDLEVvAATpTSLLISWdaPAVtVr
                  --A---   ---B---

          31        40        50        60
TNfn3     gieLTYGiKDVpGdrttIDLTedeNqySIg
FNfn10    YyrITYGeTGGnSpvqeFTVPgskStaTIs
          ---C----         --C'--    --E---

          61        70        80        90
TNfn3     NLKPDTEYeVSLiSrrG....dmSSnPaKe
FNfn10    GLKPGVDYtITVyAvtGrgdspaSSkPiSi
                -----F-----              --G

          91
TNfn3     TFtTGL
FNfn10    NyrT
          G---
```

FIGURE 1: Aligned backbone ribbon representations of (a) TNfn3 and (b) FNfn10, showing the location of the strands [produced with MOLSCRIPT (*60*)]. Panel c is a structure-based sequence alignment of TNfn3 and FNfn10 in which the conserved core residues are shaded and the strands are represented with bold letters and are labeled below the sequence. Residues in capital letters represent invariant and conservative substitutions.

fnIII domain from human fibronectin (FNfn10), consisting of 92 and 94 residues, respectively (an annotated sequence alignment is given in Figure 1, together with the structures). These domains have a very similar overall fold (the backbone rmsd between pairs of structurally equivalent residues is 1.2 Å) but a low overall level of sequence identity of ~24%. A set of 28 buried residues has been identified as the conserved hydrophobic core; these have a higher level of sequence identity (42%) and substantial structural similarity. Like other members of the immunoglobulin-like fold, TNfn3 and FNfn10 have been shown to have a similar folding nucleus (*23*, *24*). However, differences in their response to mutation and hydrogen exchange experiments have been used to infer a structural "plasticity" for FNfn10 in the A, B, and G strands (*25*). This is supported by evidence from backbone dynamics of greater chemical exchange in the A and B strands of FNfn10 (*12*). This paper reports a detailed analysis of the side-chain dynamics of these two domains based on deuterium relaxation data. The results suggest that TNfn3 has a highly dynamic, fluid-like hydrophobic core in contrast to that of FNfn10, which appears to be more rigid. The small chemical shift range and rapid $R_{1\rho}$ relaxation rates of the deuterium nucleus make its relaxation parameters insensitive to chemical exchange on a slow microsecond to millisecond time scale (*26*); additionally, it appears that since the deuterium relaxation rates sample frequencies lower than those for carbon relaxation, they are less sensitive to the time scale of molecular motion (i.e., closer to the extreme narrowing limit) and therefore provide a more robust access to methyl axial order parameters characterizing picosecond to nanosecond time scale motion than carbon relaxation (*27*).

MATERIALS AND METHODS

Sample Preparation. TNfn3 and FNfn10 were expressed from the pFN10 and pTEN1 plasmids, respectively, and purified by affinity chromatography as described previously (*28*, *29*). The "extended" 1−92 form of tenascin was used (*28*), and each protein had an N-terminal Gly-Ser dipeptide remaining after cleavage of the affinity tag. Uniformly ^{15}N-labeled and ^{13}C- and ^{15}N-labeled samples were expressed in *Escherichia coli* strain C41 cells (*30*) grown in M9 minimal medium using $^{15}NH_4Cl$ and [U-^{13}C]6-glucose as the sole nitrogen and carbon sources, respectively, as necessary. Samples for side-chain dynamics were expressed in minimal medium containing $^{15}NH_4Cl$ and [U-^{13}C]6-glucose as the sole nitrogen and carbon sources, respectively, and 65% D_2O, resulting in uniform ^{13}C and ^{15}N labeling and approximately 50% uniform deuteration. Stereospecific assignments of the methyl groups were facilitated by protein samples grown using 10% [U-^{13}C]6-glucose as the carbon source. All samples were prepared in 50 mM sodium acetate buffer at pH 5.0 in 10% D_2O, at an approximate concentration of 1−2 mM, with the exception of that for TNfn3 side-chain dynamics, which was dissolved in pure D_2O. Microbial growth was prevented by the addition of 0.05% sodium azide, and each sample was degassed and sealed.

Chemical Shift Assignments. Experiments were carried out with a Bruker AMX 500 spectrometer with ^{15}N and ^{1}H channels, and DRX 500 and DRX 600 spectrometers equipped with triple-resonance probes at 298 K. Previous backbone assignments were available for both proteins (*31*, *32*) and were confirmed with three-dimensional (3D) ^{15}N-edited TOCSY experiments. Side-chain methyl assignments were based on (H)CC(CO)NH and H(CC)(CO)NH "preceding" TOCSY experiments (*33*) together with the 3D ^{15}N-edited TOCSY experiment. Stereospecific methyl assignments were obtained from a modified ^{1}H−^{13}C HSQC spectrum for a 10% ^{13}C-labeled sample (*34*).

Backbone ^{15}N Relaxation Measurements. Backbone dynamics was determined from ^{15}N T_1 and T_2 relaxation times and the steady state heteronuclear ^{1}H−^{15}N NOE enhancement at 500 MHz. T_1 times were measured from inversion−recovery experiments with delays of 40, 80, 120, 200, 280, 360, 480, 600, 720, 840, and 1000 ms. T_2 experiments employed a CPMG pulse train with a spin-echo delay of 875 μs and relaxation delays of 7, 28, 42, 56, 70, 84, 98, 112, 126, 140, 168, and 196 ms. Presaturation in the ^{1}H−^{15}N NOE experiments employed a 120° pulse train interleaved by 5 ms delays. Relaxation delays were set to 3 and 5 s for the T_1 and T_2 experiments and the heteronuclear NOE experiments, respectively. ^{1}H−^{15}N steady state NOE enhancements were calculated as the ratio of peak volumes from spectra recorded with and without presaturation of amide proton resonances. NOE ratios were calculated from peak integrals obtained from a Lorentzian fit to each peak, and relaxation times from a single-exponential fit to peak

heights using the program Sparky (*35*). The program estimates errors in the rates by a Monte Carlo error estimation procedure in which fits are made to a set of synthetic data sets in which a random error from a Gaussian distribution is added to each peak height; the error is then obtained from the variance of fitted rates over the synthetic data sets. Errors in NOE volumes were estimated from the Lorentzian fit residual.

Data were analyzed using standard protocols for backbone dynamics (*3*) with the program TENSOR2 (*36*). The correlation time for molecular tumbling, τ_m, was determined from the trimmed mean R_2/R_1 ratio, and the data for each nucleus were fitted to the simplest form of the model-free formalism which could explain the data; this resulted in a chemical exchange term for some residues.

Side-Chain Methyl ^2H Relaxation Measurements. Deuterium relaxation times T_1(D) and $T_{1\rho}$(D) were determined by measuring the relaxation of the three- and two-spin product operator terms $I_zC_zD_z$, $I_zC_zD_y$, and I_zC_z as described by Muhandiram *et al*. (*5*). Values for the relaxation rates of $I_zC_zD_z$ and I_zC_z were obtained from series of $^1H-^{13}C$ spectra recorded with relaxation delays of 0.05, 4.5, 9.5, 15, 21, 28, 36, 45, and 57.7 ms and of $I_zC_zD_y$ from spectra with delays of 0.2, 1.3, 2.8, 4.4, 6.2, 8.4, 10.9, and 15.1 ms. Relaxation rates were fitted to the peak heights by fitting a single exponential without an offset using the program Sparky (*35*). T_1(D) and $T_{1\rho}$(D) were then obtained by correcting for the dipolar contribution to relaxation using the I_zC_z rates (*5*):

$$1/T_1(D) \approx 1/T_1(I_zC_zD_z) - 1/T_1(I_zC_z) \quad (1)$$

$$1/T_{1\rho}(\mathrm{D}) \approx 1/T_1(I_zC_zD_y) - 1/T_1(I_zC_z) \quad (2)$$

All the data were fitted to the original model-free approximation to the spectral density (*37*), given by eq 3, resulting in a value of the generalized order parameter S^2 describing the extent of the motion and the correlation time for internal dynamics, τ_e. In previous side-chain dynamics studies, this form of the spectral density has been shown to be adequate for most residues (*5*, *27*, *38*).

$$J(\omega) = \frac{2}{5}\left[\frac{S^2\tau_m}{1+\omega^2{\tau_m}^2} + \frac{(1-S)^2\tau}{1+\omega^2\tau^2}\right] \text{ where } \tau^{-1} = {\tau_m}^{-1} + {\tau_e}^{-1} \quad (3)$$

The relaxation rates R_1 and $R_{1\rho}$ are related to the spectral density via eqs 4 and 5 [it has been shown that, for the experimental conditions that were used, $R_{1\rho}$ is approximated well by R_2 (*5*)]. In these expressions, the "quadrupolar coupling constant", defined by e^2qQ/h, was taken to be 167 MHz as determined from residual dipolar coupling experiments (*39*). The model was fitted by least-squares optimization of the difference between experimental and fitted R_1 and $R_{1\rho}$ (*40*).

$$R_1 = \frac{3}{16}\left(\frac{e^2qQ}{\hbar^2}\right)^2[J(\omega_D) + 4J(2\omega_D)] \quad (4)$$

$$R_{1\rho} \approx R_2 = \frac{1}{32}\left(\frac{e^2qQ}{\hbar^2}\right)^2[9J(0) + 15J(\omega_D) + 6J(2\omega_D)] \quad (5)$$

Due to the rapid rotation of the methyl groups about their axes, the correlation function (S_{rot}^2) rapidly drops to a value close to that expected if rotation were the only type of motion, i.e., $[^1/_2(3\cos^2\theta^{-1})]^2$, where θ is the angle between the methyl averaging axis and the C−D bond. If the axial motion and rotation about the axis are independent, the overall order parameter (S^2) can be factorized as $S_{rot}^2S_{axis}^2$; for tetrahedral geometry, $S_{rot}^2 \sim 0.111$. There is experimental evidence that the angle θ is slightly larger than tetrahedral, from residual dipolar coupling experiments ($\theta = 110.9°$) and neutron diffraction ($\theta = 110.03°$ for alanine and 111.88° and 111.42° for Leu methyls $\delta1$ and $\delta2$, respectively). This would result in S_{axis}^2 values that are between 6 and 31% larger. However, since it is not known whether the unique axis of the C−D quadrupolar interaction tensor is exactly collinear with the C−D bond, and the use of a larger value of θ results in S_{axis}^2 being greater than unity for some methyl groups, the conventional value of 0.111 has been used.

Heteronuclear Coupling Measurements. Three-bond $^{13}C-^{13}C$ and $^{15}N-^{13}C$ couplings were measured using quantitative *J* correlation experiments (*41*, *42*), yielding $^3J_{C\alpha-C\delta}$, $^3J_{C\gamma-C'}$, and $^3J_{C\gamma-CN}$.

RESULTS

Assignments. Chemical shift assignments of the side chains were made using standard triple-resonance experiments. The $^1H-^{13}C$ HSQC spectrum of TNfn3 was excellently resolved (Figure 2a), allowing complete assignment of side-chain methyls and unambiguous measurement of relaxation rates. For FNfn10, a number of threonine and valine signals in the center of the methyl region of the spectrum (Figure 2b) overlap. Deuterium relaxation rates for these methyls were nonetheless measured and analyzed as usual, but they have been indicated in Table 1. Since there is no simple way to separate the contributions from overlapped peaks, the data for these methyl groups should be treated with caution. Confidence in the results for these methyls is obtained from the agreement of axial order parameters for valine γ-methyls in the overlapped region with those which are well-resolved (e.g., $\gamma1$ and $\gamma2$ of V1); it is well established that order parameters for the stereotopic methyls in valine and leucine are usually very similar (*43*). In any event, it will be seen that the results for the overlapped signals do not affect the conclusions presented below.

Fitting of Side-Chain Dynamics Data. Interpretation of the side-chain dynamics experiments depends on the determination of an isotropic molecular tumbling time, τ_m, usually obtained from backbone dynamics experiments. Backbone dynamics have been reported for both proteins (*12*), and have demonstrated that isotropic tumbling is an adequate description. The backbone dynamics experiments were repeated under the conditions described here, and the mean ^{15}N R_2/R_1 ratio for residues not undergoing exchange was used to estimate a rotational correlation time using the program Tensor2 (*36*), giving values of 6.06(2) and 6.91(2) ns for TNfn3 and FNfn10, respectively. These values are slightly larger than one set of published results [5.19 and 6.43 ns, respectively (*12*)], although larger values have previously been obtained for TNfn3 under similar conditions (*31*). Internal motional models were fitted using Tensor2 and gave excellent agreement with the earlier results (Supporting

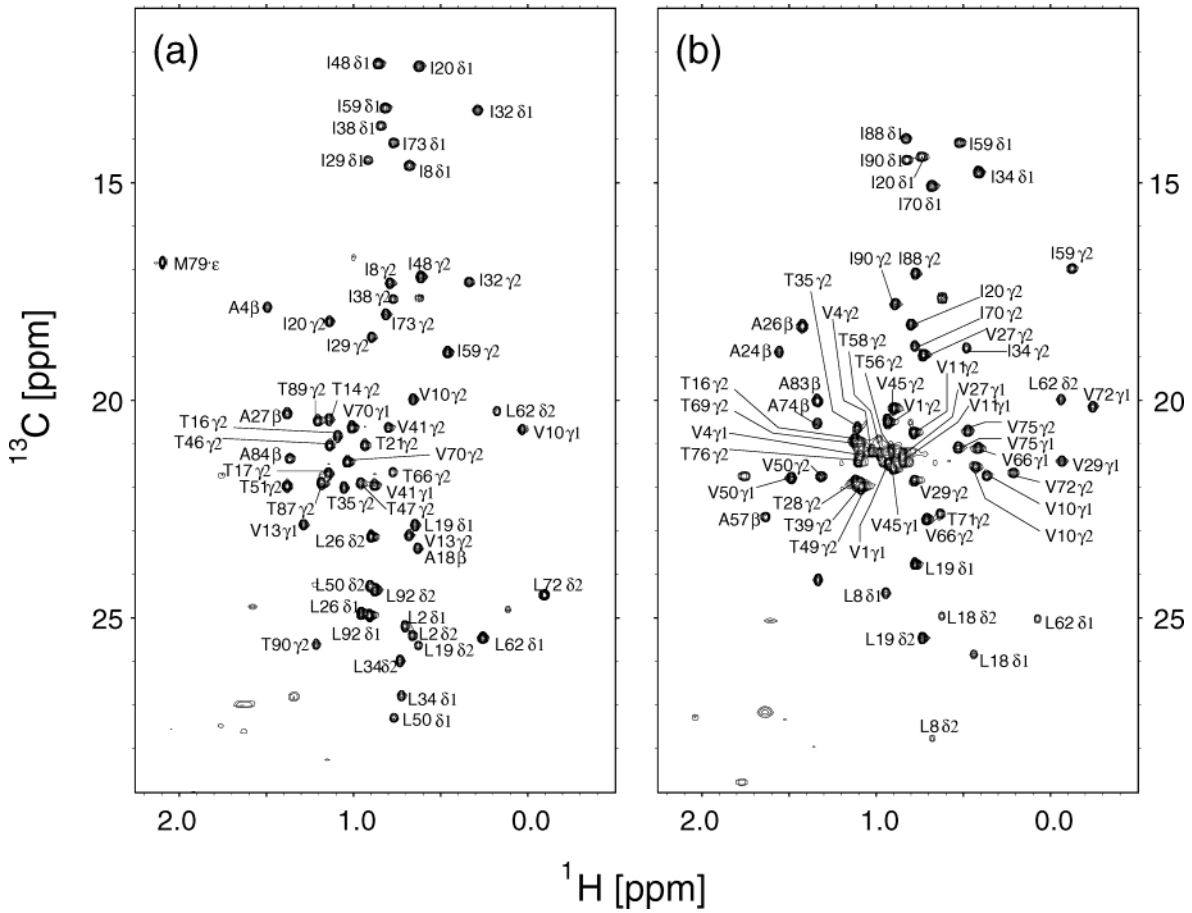

FIGURE 2: ^{1}H−^{13}C HSQC correlation maps of (a) TNfn3 and (b) FNfn10, showing the stereospecific methyl group assignments. Some crowding is seen in the central threonine/valine region for FNfn10.

Information). These show that the backbone dynamics of the two domains are essentially the same on a picosecond to nanosecond time scale, except for the FG loop (which is longer in FNfn10) and the CC′ loop.

All methyl carbon resonances in the ^{1}H−^{13}C HSQC spectrum were assigned, with the exception of A12 β, A13 β, T14 γ2, and T94 γ2 in FNfn10, and are illustrated in Figure 2 (assignments available as Supporting Information). Deuterium quadrupolar relaxation rates T_1(D) and $T_{1\rho}$(D) (Supporting Information) were fit to the original three-parameter (S^2, τ_e, and τ_m) Lipari−Szabo spectral density function with τ_m fixed to the above isotropic tumbling times, using in-house software; for TNfn3, τ_m was adjusted to 7.57 ns to account for the increased viscosity of D_2O. We have also checked τ_m by recording T_1 and T_2 relaxation times in D_2O for those amide protons which had not undergone solvent exchange (data available upon request); because of the low pH, hydrogen−deuterium exchange is relatively slow. The resulting tumbling time of 7.3 ns is close to the viscosity-corrected value determined in water and produces almost identical results for the fitted internal dynamics parameters (e.g., the largest difference in order parameter is less than 3%). Table 1 lists the fitted parameters. Errors were estimated both by Monte Carlo resampling of the data (*40*) and from the (computationally cheaper) fit covariance matrix, giving almost identical results. Only the results from the covariance matrix are shown. In all cases, errors on the fitted parameters were less than 10% (usually much less), with the exception of L18 δ2 of FNfn10 which is a low-intensity peak and gave large errors in the fitted relaxation rates. The fitted relaxation parameters were within two standard deviations (95% confidence level) of the experimental values in all cases except T35 γ2 in TNfn3 and A57 β, I70 γ2, and V27 γ2 in FNfn10. All axial order parameters took on physically sensible values between 0 and 1, within error.

The interpretation of the effective correlation times, τ_e, is not straightforward (*27*), as they tend to be dominated by the contribution of methyl spinning rather than axis motion. The distributions of methyl axial order parameters, shown in Figure 3, are broadly similar to those for other proteins. Alanine β-methyls are constrained by their proximity to the backbone, and all have high order parameters. In fact, a significant correlation of side-chain methyl and amide N−H order parameters is observed for alanine residues (correlation coefficient of 0.78), despite the intervening Φ angle. Similarly, threonine γ2-methyls are relatively restricted in motion, probably due to limits in the hydroxyl group orientation. All other types of methyls have more heterogeneously distributed order parameters (notably valines in TNfn3), emphasizing the importance of the local environment. In general, δ-methyls have lower order parameters than γ-methyls, which are in turn lower than those of β-methyls. However, there is no simple correlation with structural properties. The distance to the surface or the solvent accessible surface area shows little correlation with order parameters, while using the number of heavy atom contacts (within 6.0 Å) made by the methyl carbon results in a correlation coefficient of ~0.5. The global order parameter

Table 1: Fitted Axial Order Parameters, S_{axis}^2, and Correlation Times, τ_e, for Each Protein

TNfn3			FNfn10		
methyl	S_{axis}^2	τ_e (ps)	methyl	S_{axis}^2	τ_e (ps)
L2 δ1	0.22 (0.01)	75.8 (1.7)	V1[a] γ1	0.16 (0.01)	69.6 (2.3)
L2 δ2	0.32 (0.04)	94.3 (2.6)	V1 γ2	0.16 (0.01)	52.2 (1.3)
A4 β	0.85 (0.00)	22.0 (0.3)	V4[a] γ1	0.62 (0.02)	90.4 (2.7)
I8 δ1	0.37 (0.01)	39.7 (0.4)	V4[a] γ2	0.61 (0.09)	70.4 (3.4)
I8 γ2	0.69 (0.02)	57.3 (1.0)	L8 δ1	0.64 (0.05)	49.4 (5.0)
V10 γ1	0.73 (0.03)	26.3 (0.6)	V10 γ1	0.85 (0.03)	76.9 (3.4)
V10 γ2	0.74 (0.02)	25.3 (0.8)	V10 γ2	0.77 (0.03)	31.0 (0.9)
V13 γ1	0.74 (0.07)	64.6 (1.5)	V11[a] γ1	0.42 (0.06)	81.9 (1.6)
V13 γ2	0.88 (0.05)	13.1 (1.5)	V11 γ2	0.36 (0.03)	62.0 (1.3)
T14 γ2	0.83 (0.01)	83.4 (0.7)	T16[a] γ2	0.98 (0.01)	53.2 (2.1)
T16 γ2	1.03 (0.02)	72.4 (0.6)	L18 δ1	0.35 (0.05)	67.2 (3.0)
T17 γ2	0.80 (0.02)	64.0 (0.9)	L18 δ2	0.42 (0.45)	49.4 (24.1)
A18 β	0.75 (0.01)	90.0 (1.4)	L19 δ1	0.29 (0.01)	36.8 (1.2)
L19 δ1	0.56 (0.02)	32.4 (1.0)	L19 δ2	0.35 (0.01)	47.3 (2.2)
L19 δ2	0.54 (0.03)	51.6 (0.9)	I20 δ1	0.71 (0.03)	20.3 (1.6)
I20 δ1	0.36 (0.01)	36.8 (0.3)	I20 γ2	0.73 (0.02)	26.0 (1.4)
I20 γ2	0.73 (0.01)	34.5 (0.6)	A24 β	0.84 (0.02)	58.3 (1.7)
T21 γ2	0.72 (0.02)	66.7 (2.7)	A26 β	0.77 (0.01)	40.6 (2.5)
L26 δ1	0.15 (0.01)	49.8 (0.5)	V27 γ1	0.40 (0.01)	80.5 (2.3)
L26 δ2	0.19 (0.01)	43.1 (0.6)	V27[a] γ2	0.44 (0.01)	59.6 (0.9)
A27 β	0.67 (0.00)	50.4 (0.5)	T28[a] γ2	0.55 (0.03)	56.6 (3.3)
I29 δ1	0.79 (0.03)	22.5 (0.7)	V29 γ1	0.85 (0.02)	75.4 (2.9)
I29 γ2	0.73 (0.03)	57.9 (0.9)	V29 γ2	0.73 (0.03)	43.6 (2.8)
I32 δ1	0.63 (0.01)	29.8 (1.1)	I34 δ1	0.08 (0.01)	32.1 (0.7)
I32 γ2	0.68 (0.02)	75.8 (0.9)	I34 γ2	0.95 (0.04)	41.6 (1.3)
L34 δ1	0.34 (0.02)	59.0 (3.7)	T35 γ2	0.89 (0.03)	40.8 (3.4)
L34 δ2	0.27 (0.01)	48.7 (0.5)	T39[a] γ2	0.74 (0.03)	55.8 (1.9)
T35 γ2	0.71 (0.03)	78.5 (0.5)	V45[a] γ1	0.40 (0.01)	55.8 (0.6)
I38 δ1	0.72 (0.02)	23.3 (1.0)	V45 γ2	0.49 (0.01)	40.6 (1.0)
I38 γ2	0.78 (0.01)	100.5 (1.8)	T49[a] γ2	0.67 (0.13)	69.5 (5.5)
V41 γ1	0.76 (0.06)	35.5 (1.4)	V50 γ1	0.45 (0.01)	89.8 (1.1)
V41 γ2	0.95 (0.06)	51.4 (1.0)	V50 γ2	0.44 (0.02)	95.2 (1.7)
T46 γ2	0.69 (0.01)	74.7 (2.0)	T56[a] γ2	0.56 (0.02)	60.2 (2.0)
T47 γ2	0.83 (0.01)	63.1 (1.0)	A57 β	0.92 (0.03)	39.3 (4.5)
I48 δ1	0.22 (0.00)	34.5 (0.3)	T58 γ2	0.72 (0.03)	71.2 (2.5)
I48 γ2	0.47 (0.01)	57.7 (0.6)	I59 δ1	0.53 (0.03)	25.9 (0.9)
L50 δ1	0.47 (0.09)	48.4 (3.8)	I59 γ2	0.74 (0.03)	41.4 (0.9)
L50 δ2	0.52 (0.07)	40.5 (6.4)	L62 δ1	0.69 (0.06)	47.2 (5.1)
T51 γ2	0.63 (0.02)	46.4 (0.5)	L62 δ2	0.80 (0.02)	20.2 (1.4)
I59 δ1	0.27 (0.01)	46.5 (0.4)	V66 γ1	0.74 (0.02)	108.5 (3.4)
I59 γ2	0.27 (0.01)	86.1 (1.3)	V66 γ2	0.70 (0.03)	51.7 (1.7)
L62 δ1	0.72 (0.02)	78.1 (4.5)	T69[a] γ2	0.91 (0.02)	57.8 (2.1)
L62 δ2	0.75 (0.03)	24.6 (0.9)	I70 δ1	0.36 (0.02)	24.4 (1.3)
T66 γ2	0.86 (0.06)	124.2 (0.6)	I70 γ2	0.84 (0.04)	36.9 (1.6)
V70 γ1	0.12 (0.01)	73.9 (0.7)	T71 γ2	0.92 (0.11)	81.9 (6.3)
V70 γ2	0.12 (0.01)	83.6 (0.9)	V72 γ1	0.82 (0.02)	50.8 (1.6)
L72 δ1	0.25 (0.01)	47.0 (1.0)	V72 γ2	0.86 (0.05)	30.5 (2.2)
L72 δ2	0.25 (0.02)	56.8 (0.5)	A74 β	0.93 (0.03)	38.0 (4.3)
I73 δ1	0.46 (0.01)	27.2 (0.8)	V75 γ1	0.90 (0.04)	46.6 (2.4)
I73 γ2	0.63 (0.01)	58.2 (0.3)	V75 γ2	0.90 (0.02)	26.7 (1.3)
M79 ϵ	0.05 (0.01)	14.4 (0.3)	T76[a] γ2	0.80 (0.06)	67.9 (3.9)
A84 β	0.82 (0.01)	116.9 (2.2)	A83 β	0.69 (0.01)	51.0 (1.4)
T87 γ2	0.46 (0.02)	85.0 (1.8)	I88 δ1	0.55 (0.02)	29.9 (1.8)
T89 γ2	0.75 (0.03)	61.7 (1.3)	I88 γ2	0.58 (0.03)	49.9 (1.3)
T90 γ2	0.96 (0.01)	92.3 (3.1)	I90 δ1	0.63 (0.02)	21.0 (1.2)
L92 δ1	0.14 (0.03)	33.1 (1.0)	I90 γ2	0.80 (0.04)	53.6 (1.4)
L92 δ2	0.10 (0.02)	31.2 (1.3)			

[a] Overlapped threonine and valine residues.

distribution is broad, but it does not form the trimodal pattern found by Lee *et al.* (*21*), regardless of how the data are binned.

Spatial Distribution of Order Parameters. Figure 4 shows the methyl order parameters projected onto the aligned protein structures (panels a and b). As noted before, it is immediately obvious that there is no simple relation of order parameter to depth of burial. The terminal residues and the methionine (in TNfn3) have low order parameters, but several other surface residues, even in loops, have relatively high order parameters (witness A27 and V27 in TNfn3 and FNfn10, respectively). What does stand out, though, is that within the core of TNfn3 there is a cluster of deeply buried residues with unusually low order parameters, with an increase in order parameters as one moves away from the center of the core. In FNfn10, the core is apparently much more rigid, with most order parameters being above 0.6. If anything, the opposite trend is seen, in which the periphery is more mobile than the center of the hydrophobic core.

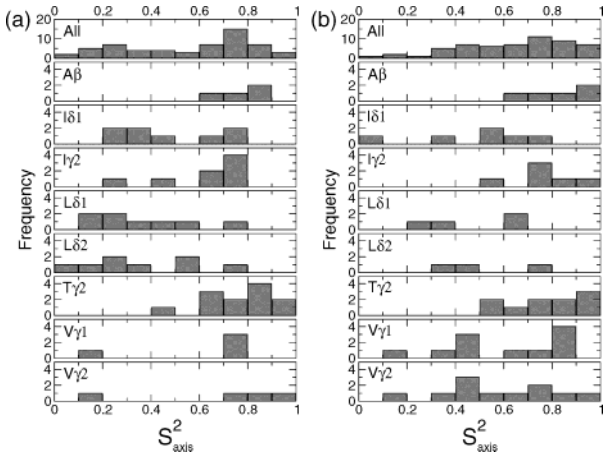

FIGURE 3: Axial order parameter distributions of (a) TNfn3 and (b) FNfn10. The top panel shows the overall distribution of all order parameters, while the remainder are classified by methyl type.

Panels c and d of Figure 4 show the core order parameters only, in an exploded schematic view of the core. The most deeply buried residues of the TNfn3 core (V70, L72, I48, I59, I20, and I8) all display high mobility, especially residue 70 whose order parameters lie well below the expected range for a valine. Peripheral residues (e.g., A84, I32, I29, L50, L62, A18, and V10) are significantly less mobile. With the exception of I34 δ1, the core methyls of FNfn10 are much less mobile (compare I70 with V70 in TNfn3 or I59 with that in TNfn3) and do not show the continuous decrease in mobility from the center of the core seen for TNfn3.

Although visual inspection of the structures and schematics may suggest that there is a correlation between order parameters for residues which are close in space, a calculation for these proteins showed that this correlation only persists over a short distance so that order paramters are only correlated for residues which are essentially in contact with one another. Of the three residues with the lowest order parameters in TNfn3, I59 and V70 are close (minimum separation of 3.33 Å), while the I48−I59 and I48−V70 distances are 4.90 and 7.48 Å, respectively.

Comparison of TNfn3 and FNfn10 as Homologous Domains. It is difficult to compare domains with a low level of sequence identity due to the different residues in aligned positions, particularly when one is measuring a side-chain property. As Figure 3 demonstrates, the amino acid type strongly influences the side-chain order parameters. The limited number of aligned residues in TNfn3 and FNfn10 that are identical generally have similar order parameters (V10 γ1 and γ2, T16 γ2, I20 γ2, T35 γ2, and L62 δ1 and δ2), notable exceptions being L19 δ1 and δ2, I59 δ1 and δ2, and I20 δ2. Of these, I20 and I59 are deeply buried and have lower axial order parameters in TNfn3, supporting the

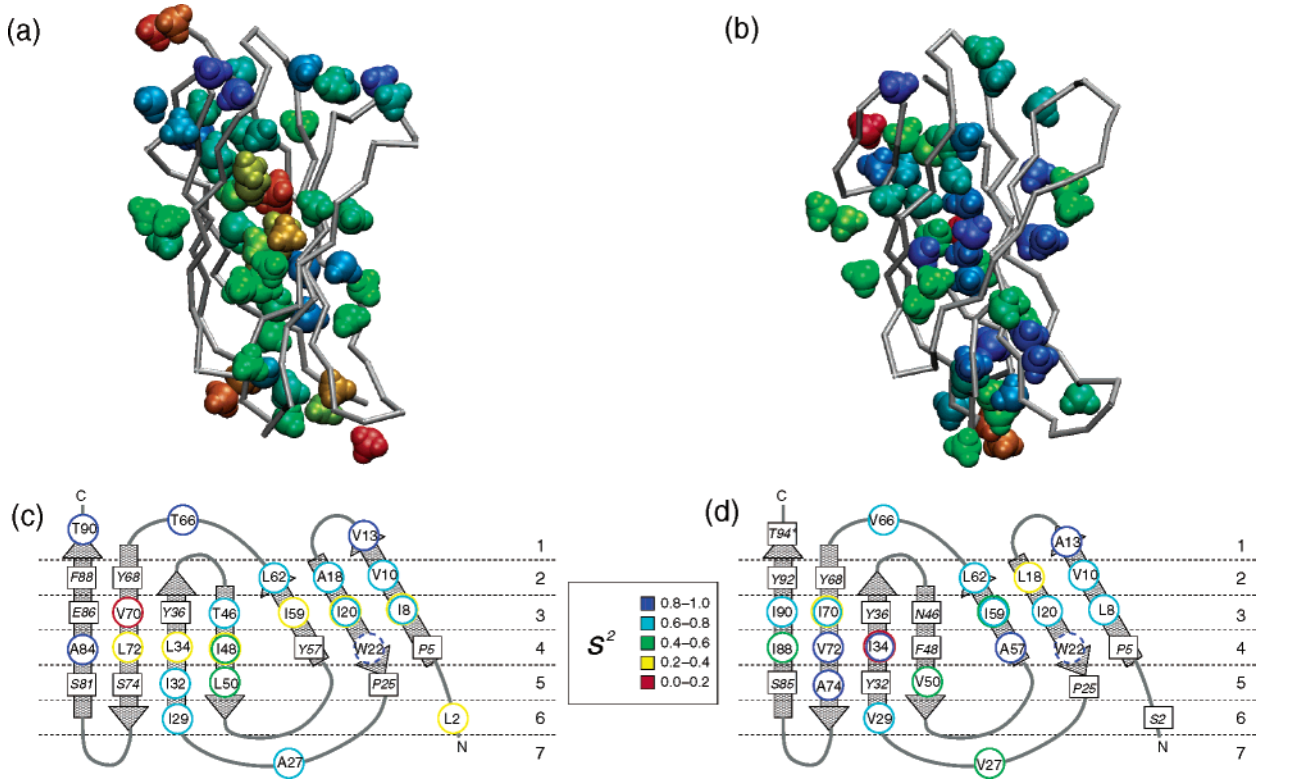

FIGURE 4: Spatial distribution of order parameters. Order parameters of each methyl group are mapped onto the structures of (a) TNfn3 and (b) FNfn10. Methyls are colored from red (order parameters of zero) to blue (order parameters of unity). A schematic view showing just the hydrophobic core residues is presented in panels c and d for TNfn3 and FNfn10, respectively, with a similar color scale. In TNfn3, the residues at the center of the core are significantly more mobile than those at the periphery. In FNfn10, the center of the core is less mobile than the peripheral regions.

hypothesis that the core of TNfn3 is more dynamic than that of FNfn10. L19 is more flexible in FNfn10, but is close to the surface.

To compare residues in other positions, it was necessary to normalize the order parameters by some means. Eight proteins for which both published data and structures are available were selected: the N-terminal SH3 domain from the *Drosophila* adaptor protein drk (drkN SH3) (*44*), the C-terminal SH2 domain from phospholipase $C_{\gamma 1}$ (PLCC SH2) (*5*, *18*), the SH2 domain of the SAP protein (*17*), ubiquitin (*6*), oxidized flavodoxin (*45*), fatty acid binding proteins A-LBP and M-FABP (*13*), and calmodulin (*20*). From this data set, averages and standard deviations were calculated for order parameters for each kind of methyl group. It is then possible to normalize the order parameters of TNfn3 and FNfn10 by calculating a *Z* score, namely, the number of standard deviations the order parameter is away from the mean for that type of residue. Since it is known that the order parameters do not come from a Gaussian distribution (*43*), no statistical significance can be attached to the value of *Z*, but the values provide a means of qualitative comparison. Figure 5 compares these *Z* scores for TNfn3 and FNfn10, highlighting the outlying data. While many data points lie within or close to one standard deviation of the mean, there are several significant outliers. One type is at the termini, which have unusually low order parameters, but that is not unexpected. In FNfn10, there are a few other low outliers, but mostly on the surface or in loops: V11 on the surface of the {A,B,E} sheet, V27 in the BC loop, V45 in the CC′ loop, A83 in the FG loop, and I88 in the peripheral G strand. Only I34 $\delta 1$ is deeply buried in the hydrophobic

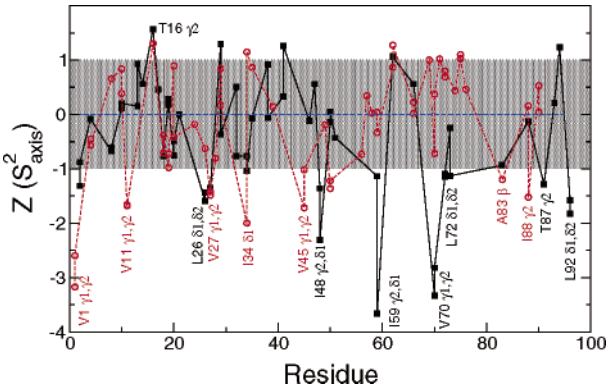

FIGURE 5: *Z* scores for S_{axis}^2 for TNfn3 (black lines and filled black squares) and FNfn10 (red lines and empty red circles). Residues with outlying *Z* scores have order parameters significantly different from the mean for that residue type. These are labeled in black for TNfn3 and red for FNfn10. In FNfn10, all outliers with low *Z* scores are mobile surface or terminal residues (V1, V11, V27, V45, A83, and I88), with the sole exception being I34 $\delta 1$. In TNfn3, four outliers are deeply buried in the core of the protein (I48, I59, V70, and L72), and several of these are many standard deviations below the expected order parameter for that kind of residue.

core; however, inspection of the pattern of order parameters in Figure 4 shows that it is an isolated case. By contrast, TNfn3 has a number of buried core residues with significantly low order parameters, namely, I48 $\gamma 2$ and $\delta 1$, I59 $\gamma 2$ and $\delta 1$, V70 $\gamma 1$ and $\gamma 2$, and L72 $\delta 1$ and $\delta 2$, the *Z* scores for V70 and I59 being particularly low. Thus, not only are the order parameters of most methyl groups in the TNfn3 core generally low, but there are several which lie well below the statistically expected range; this is very rarely seen for

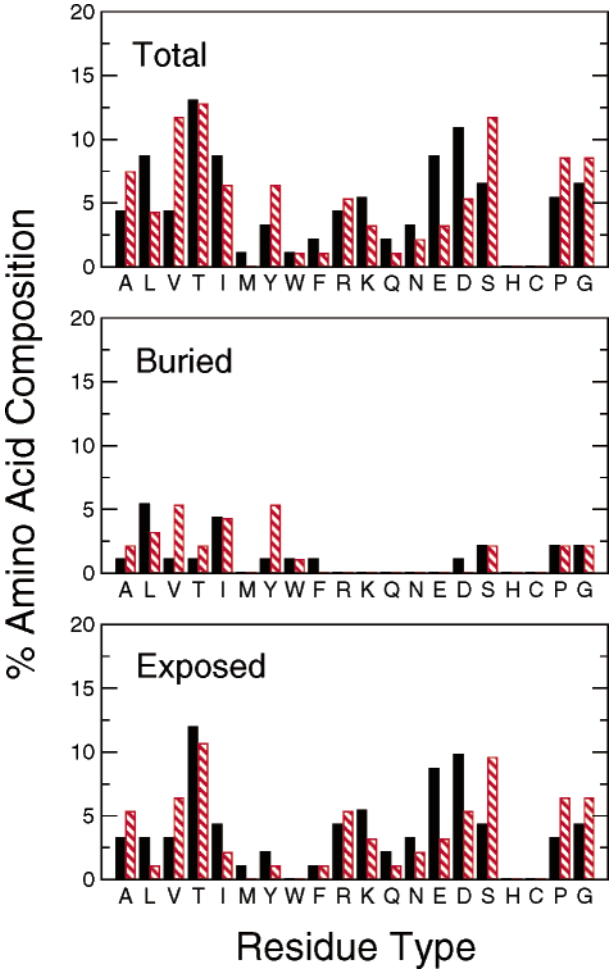

FIGURE 6: Amino acid composition of TNfn3 (filled black bars) and FNfn10 (hatched red bars). Buried amino acids are defined as those with less than 10% exposed surface area. FNfn10 has more valine and tyrosine residues, whereas TNfn3 has more leucines.

buried residues in other proteins for which this approach has been applied.

Relation of Dynamics to Core Composition. What is the effect of the overall core composition of the two proteins on their dynamics? Figure 6 shows the amino acid residue composition of each protein. The low level of sequence homology of these domains is reflected in their different overall composition, with TNfn3 having many more acidic residues. For the hydrophobic core (defined as amino acids with less than 10% exposed surface area), there is a similar content of alanine, isoleucine, serine, proline, and glycine in both proteins. However, TNfn3 has more leucines (six vs three for FNfn10), while FNfn10 has more valines (six vs one for TNfn3) and more tyrosines (six vs one for TNfn3). The longer γ-branched side chain of leucine would be expected to result in a more dynamic core than β-branched valine, and tyrosine, being a bulky aromatic, ought to reduce core mobility. As a result, the global core composition of TNfn3 would be expected to cause greater mobility, possibly reducing the order parameters of its side chains to values lower than those they would normally take.

Relation of Dynamics to Packing Density. Another possible contribution to core mobility is the amount of buried "free volume" in which the side chains can move, or packing density. One method of measuring free volume is to do a grid search for points outside of any atom and within the

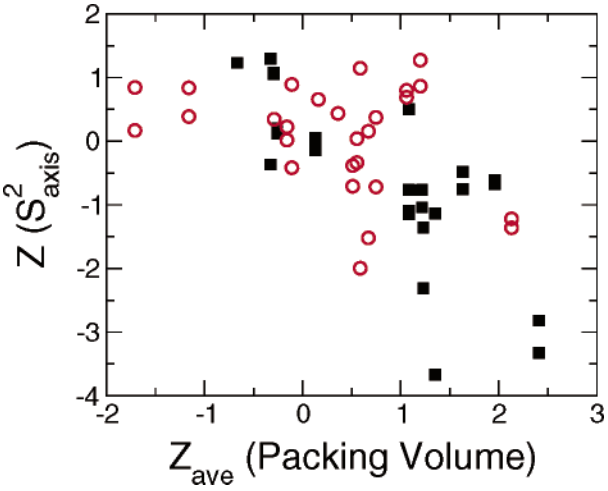

FIGURE 7: Correlation between *Z* scores for order parameters and *Z* scores for excess packing volume (TNfn3 data are given as filled black squares and FNfn10 data as empty red circles). The order parameter *Z* scores indicate how many standard deviations each order parameter is from the mean for that type of methyl group; the packing volume *Z* scores (*48*) indicate the mean number of standard deviations the volumes assigned to atoms in that residue are from the means calculated from the Protein Data Bank. The TNfn3 data are systematically shifted to larger *Z* scores for packing density and smaller for order parameters.

core, although this raises the issue of how to objectively define the core. A search was made over a 0.5 Å grid for points which lay outside all atoms, but within 2.0 Å of the set of core residue side chains shown in panels c and d of Figure 4, giving free volumes of 118.1 and 96 Å^3 for crystal structures of TNfn3 [PDB entry 1TEN (*46*)] and FNfn10 [PDB entry 1FNF (*47*)], respectively (structures were initially minimized in the CHARMM 19 potential to reduce the dependence on crystal structure quality and crystal packing effects). Alternatively, packing can be assessed by the construction of Voronoi polyhedra around the core atoms, which eliminates the problem of defining the core volume, as it is determined by neighboring atoms. One such method is that implemented in the program PROVE (*48*), in which the volume distribution for each atom type has been computed for a large sample of crystal structures. The excess packing volume of each buried atom may then be determined as a *Z* score using these statistics, positive values indicating "underpacking" and negative values "overpacking". When this method is applied to the minimized crystal structures, total excess volumes of 105.8 and 42.9 Å^3 are obtained for TNfn3 and FNfn10, respectively; both methods of assessing free volume suggest that the core of TNfn3 is less densely packed.

A mean excess volume *Z* score can also be computed over all the side-chain atoms of a residue, and Figure 7 shows the relation between the *Z* scores for order parameters described above and the volume *Z* scores for all core residues for which side-chain dynamics data were obtained. There is clearly a negative correlation for TNfn3 (correlation coefficient of −0.75), showing that an excess packing volume for a side chain results in lower than expected order parameters. For FNfn10, the correlation is much poorer (correlation coefficient of −0.34), but the distribution of values is narrower in that case. Packing volume is only one possible effect in explaining the differences in dynamics, so some scatter is expected. A potential caveat when interpreting

packing *Z* scores is that they can reflect the quality of the crystal structure (the motivation for developing the method). However, structures were minimized in the same force field in an attempt to avoid this problem. In addition, computing scores for a different FNfn10 crystal structure [PDB entry 1FNA (*49*)] resulted in similar results (not shown).

The correlation of order parameter and packing volume is not the only interesting feature of Figure 7a. There is a notable shift in the TNfn3 data toward higher excess packing volumes and lower order parameters relative to the FNfn10 data, supporting the hypothesis that TNfn3 has a more dynamic core, and not only for the obviously exceptional residues.

An alternative measure of packing density is the number of nonbonded heavy atom contacts within a certain radius of the methyl of interest. In a recent study by Halle (*50*), it was shown that the mean square atomic fluctuations of heavy atoms in protein crystal structures were approximately inversely proportional to the number of nonbonded heavy atom contacts. However, the correlation of order parameter *Z* scores with the reciprocal of the number of nonbonded heavy atom contacts within 6.0 Å of the methyl carbon is much poorer than that with packing volume *Z* scores (correlation coefficients of −0.44 for TNfn3 and −0.18 for FNfn10).

Contribution of Rotameric Transitions to Side-Chain Mobility. It has recently been shown that rotamer transitions play an important role in lowering side-chain order parameters (*51*): with regard to the order parameters of side-chain γ-methyls, a significant population of alternative rotamers give rise to low order parameters. We have measured three-bond carbon−carbon and carbon−nitrogen couplings using standard quantitative *J* coupling experiments (*41*, *42*). Table 2 lists values of $^3J_{C\gamma-CN}$ and $^3J_{C\gamma-CC'}$ for valine and isoleucine residues: these data report on the side-chain χ_1 torsion angle, yielding two couplings for isoleucines and four for valines. Most of the values are approximately consistent with a single rotamer (although a small population of alternate rotamers would also be consistent with these data), and the χ_1 dihedral angles deduced from the scalar coupling data are generally in agreement with those from the crystal structures. A few residues in each protein are inconsistent with the couplings expected for a single, staggered rotamer. In TNfn3, these are V10, I48, I59, and V70, of which the latter three have low order parameters for their γ-methyls, as described above. In FNfn10, V4, V11, and V50 probably involve some rotamer averaging; V4 has unusually low γ-methyl order parameters. All three of these valines are either on the surface (V4 and V11) or on the periphery of the core (V50).

Table 2: Three-Bond Scalar Couplings (hertz) for Isoleucine and Valine Side Chains[a]

residue	$J_{NC\gamma1}$	$J_{NC\gamma2}$	$J_{C'C\gamma1}$	$J_{C'C\gamma2}$	χ_1[c]	χ_1 (crystal)[d]
TNfn3						
I8		2.3 (0.1)			−60	−58
V10	1.6 (0.1)	1.2 (0.1)		2.7 (0.3)	*b*	179
V13	2.2 (0.1)	0.6 (0.3)		3.1 (0.3)	180	180
I20		2.2 (0.1)			−60	−45
I29		0.4 (0.3)		3.2 (0.3)	60	54
I32		1.6 (0.1)			−60	−61
I38		2.2 (0.1)			−60	−65
V41	2.1 (0.1)			2.6 (0.3)	180	174
I48		0.9 (0.1)			*b*	−48
I59		1.2 (0.1)		2.0 (0.3)	*b*	−53
V70	1.3 (0.1)	1.2 (0.0)		2.8 (0.3)	*b*	61/−64
I73		0.4 (0.3)		2.5 (0.3)	60	−75
FNfn10						
V1	0.6 (0.2)	1.4 (0.1)	1.0 (0.3)		60	154
V4	1.5 (0.1)	1.2 (0.2)	0.5 (0.3)	0.5 (0.3)	*b*	−173
V10	2.2 (0.2)			3.3 (0.3)	180	171
V11	0.6 (0.2)		2.7 (0.3)	*e*	*b*	161
I20		1.3 (0.2)		4.4 (0.3)	60	64
V27	0.9 (0.2)	0.6 (0.2)	2.7 (0.3)	1.8 (0.3)	−60	−69
V29	1.6 (0.2)	0.7 (0.3)		*e*	180	−176
I34		1.5 (0.4)			−60	−65
V45	0.6 (0.2)		3.42 (0.3)		−60	−64
V50	1.1 (0.1)		2.1 (0.3)	2.1 (0.3)	*b*	174
I59		1.7 (0.2)			−60	−55
V66	2.0 (0.1)	0.4 (0.4)		2.8 (0.3)	180	172.3
I70		1.9 (0.2)			−60	−50
V72	1.6 (0.2)			3.2 (0.3)	180	−179
V75	1.7 (0.2)			2.7 (0.3)	180	177
I88		1.0 (0.2)			−60	170
I90				2.9 (0.3)	60	57

[a] Missing data correspond to couplings that were too small to be measured. [b] Scalar couplings for these residues are not consistent with a single staggered rotamer and may arise from averaging over several rotamers or from nonstaggered rotamers. [c] These values of χ_1 were deduced from scalar couplings. [d] These values of χ_1 were calculated from crystal structures 1TEN and 1FNF for TNfn3 and FNfn10, respectively. [e] Couplings could not be determined because of signal overlap.

DISCUSSION

As has been found previously, there is no simple correlation of side-chain order parameters with structural properties. Side-chain order parameters agree in their general distribution with other published values. It has been found (*21*) that the order parameters of several proteins are roughly trimodally distributed, leading to the suggestion that there may generally be three classes of motion in all proteins. However, neither TNfn3 nor FNfn10 order parameters formed a trimodal distribution, although their distributions are broad and are certainly not Gaussian. Clearly, the factors contributing to this distribution are complex, including the amino acid composition and types of motion which the different side chains in the protein undergo.

Several studies have noted that buried side chains are generally more restricted and have higher axial order parameters. The order parameter *Z* scores may be used to assess the deviation of order parameters from the mean. It is difficult to interpret these in a statistically quantitative way, which would require a knowledge of the true order parameter distribution, but for other proteins for which data have been published, it is relatively rare for buried residues to lie more than one standard deviation from the mean. Those that do are generally exposed residues on the surface or in loops. Although FNfn10 may fit this picture, TNfn3 is a clear exception. The most buried residues in the hydrophobic core are among the least restricted in this protein, some of them many standard deviations below the expected order parameter for their residue type. How is this possible? One explanation could be that the larger number of flexible residues in the TNfn3 core effectively makes it more fluid-like, thus lowering the order parameters of all involved side chains. The residue composition of the two proteins supports this hypothesis, TNfn3 having more buried leucine residues and FNfn10 more valines and tyrosines. A study of barnase side-chain dynamics using MD simulations for barstar has found

a very dynamic core, which was also attributed principally to core composition (*52*).

It appears furthermore that packing volume has a role to play in core dynamics, at least for these proteins. There is a significant correlation of packing volume *Z* score with order parameter *Z* score. Notably, the central core residues of TNfn3 which have unusually low order parameters have larger than expected packing volumes, and in general, the core of the protein is less densely packed than FNfn10. The weakness of the correlation suggests that other factors are also important, however. For example, a recent study has found a good correlation between normalized order parameters similar to ours and sequence conservation; that is, more highly conserved residues are generally more motionally restricted (*53*). This intriguing observation may be partially related to the fact that the most structurally conserved residues tend to be the most deeply buried: for our two examples the burial, as measured by the number of heavy atom contacts within 6.0 Å of the residue, and the residue preference, as defined in the above work (*53*), are significantly correlated (Spearman correlation coefficients r_s of 0.43 and 0.62 for TNfn3 and FNfn10, respectively). There is a significant correlation between the residue preference and normalized order parameter for FNfn10 ($r_s = 0.44$), but that for TNfn3 is much weaker ($r_s = 0.07$). This is mainly due to the exceptionally mobile residues in TNfn3 which appear as outliers; exclusion of these residues improves the correlation coefficient to 0.49.

Since dynamics is often inferred from crystal structures, it is interesting to compare the side-chain dynamics data with crystallographic results. For example, alternative conformations are evidence of different rotamers, although the rotamers would usually need to be of approximately equal populations to justify modeling them separately in the crystal structure solution. There is only one such case among the core residues of either protein, V70 of TNfn3, which is 46 and 54% in $g+$ and $g-$ conformations [defined according to IUPAC−IUBMB−IUPAB recommendations (*54*)], respectively. This is in accord with the unusually low order parameters for the methyl groups in this buried valine, from which multiply occupied rotamers might be expected. For FNfn10, although there are no alternative crystallographic conformers, there are two crystal structures, 1FNF (*47*) and 1FNA (*49*). Of the buried residues, only three are in different conformations in the two structures. If one specifies the side-chain conformation with the notation r_1r_2, where r_1 and r_2 are the rotamers for torsion angles χ_1 and χ_2, respectively, L18 is $g-t$ in 1FNF and $g+g+$ in 1FNA, I34 is $g-g+$ in 1FNF and $g-t$ in 1FNA, and I88 is *tt* in 1FNF and $g+t$ in 1FNA. I88 is in the G strand, and is therefore likely to be affected by the absence of most of the opposing A strand in the 1FNA structure. However, the order parameters of L18 are quite low (0.35 and 0.42), and the very low δ1-methyl order parameter (0.08) relative to the γ2-methyl order parameter (0.95) in I34 is consistent with the rotation about the χ_2 angle seen in the crystal structures. This sort of comparison is by nature anecdotal, but the crystal structures are nevertheless in accord with the side-chain order parameters and suggest that side-chain dihedral transitions are important in explaining order parameters. The importance of multiple rotamers is confirmed by the measurement of three-bond scalar couplings by NMR, which suggest that the couplings from several of the buried residues in TNfn3 with low order parameters (I48, I59, and V70) may result from rotamer averaging.

On a picosecond to nanosecond time scale, the backbone dynamics of TNfn3 and FNfn10 in secondary structure elements are essentially the same, as found here and previously. Thus, the backbone of fibronectin type III domains acts as an independent scaffold whose motion, on this time scale at least, is quite insensitive to the details of the underlying sequence; these proteins are particularly good examples, since they have such a low level of sequence homology. Moreover, there are many other backbone dynamics studies of other homologous domains which include similar findings, suggesting that this is a general property of a fold, and not specific to the fibronectin type III superfamily. By contrast, deuterium side-chain dynamics experiments, which are most sensitive to motion on this time scale, reveal that side-chain dynamics is much more heterogeneous, and hence a more useful reporter on native state properties such as residual entropy, which could conceivably vary substantially from protein to protein, even if they have the same overall topology (*20*). TNfn3 and FNfn10 are outstanding examples of the variety of core mobility which is possible in the same fold.

The relation between side-chain dynamics and the residual entropy of the native state has been noted (*21*). However, the residual entropy measured by side-chain dynamics experiments is only a part of the total native state entropy which is in turn part of the total free energy of the native state (*55*), so it is not possible to make a simple connection between the dynamics probed by NMR and overall thermodynamics. In fact, it is FNfn10 which is the more stable of the two proteins, having a free energy for unfolding of 9.4 kcal/mol compared to a value of 6.7 kcal/mol for TNfn3 (*28*, *56*), despite having the less flexible core. One possible explanation for this could be a larger loop entropy for FNfn10 (suggested by the backbone dynamics of the FG and CC′ loops) which could compensate for the difference in core entropy. Furthermore, there are enthalpic contributions, for example, from core packing, and effects of the different protein surfaces (*57*) and possible differences in solvation free energy (*58*, *59*). Finally, when stabilities are compared, the possibility of differential effects in the denatured state must also be considered.

A degree of structural plasticity in the A, B, and G strands has earlier been ascribed to FNfn10 due to its propensity to accommodate mutations in these regions of structure, and also due to backbone chemical exchange and hydrogen exchange measurements by NMR. The side-chain order parameters provide no evidence of this: the order parameters in these regions of structure all lie within the expected range for the residues that are involved, and FNfn10 appears to have the less dynamic core. It is possible that FNfn10 is able to accommodate mutations through an increase in the entropy of its more rigid core, but this explanation seems unlikely given the large number of other proteins with similar core mobility which respond as expected to mutation, and as observed above, such interpretations need to be made cautiously. Of course, side-chain dynamics is mainly sensitive to fast time scale motions, and the backbone chemical exchange suggests that a slower millisecond to microsecond time scale may be involved. Recently developed relaxation−

dispersion experiments now permit the measurement of the rate of exchange in side chains and have revealed exchange rates on the order of microseconds for core residues of the proteins that have been studied. The use of such methods may shed further light on the plasticity in FNfn10.

Nonetheless, the insensitivity of deuterium relaxation to slower time scale motions makes it ideal for comparison with computer simulations. Molecular dynamics simulations can usually only be run for nanoseconds, but this ought to be sufficient to capture the observed side-chain motions, and to provide further mechanistic details about the core mobility: we are currently pursuing this work.

CONCLUSION

Deuterium side-chain dynamics experiments have been run on homologous fibronectin type III domains TNfn3 and FNfn10. Methyl axial order parameters show that the cores of the two proteins are quite different, that of TNfn3 being much more dynamic, with a gradual decrease of order parameters toward the center of the protein, while that of FNfn10 has more uniform dynamics, and is more rigid. Although the core residues of TNfn3 would be expected to have lower order parameters since there are more leucines and few valines, it turns out that they are even significantly lower than expected for these types of residue, suggesting that the core composition cooperatively lowers the degree of order in the core, making it more fluid-like. In addition, there is evidence that core packing density has an effect on core dynamics, especially in TNfn3.

The backbone dynamics of these domains, and of other examples, shows that backbone dynamics on a fast picosecond to nanosecond time scale is mostly determined by the fold topology. This example of side-chain dynamics demonstrates that a single fold is able to accommodate a wide range of core dynamics. The generality of this conclusion, and the causes identified here, would naturally need to be tested on other proteins of related structure, but the examples chosen here are good representatives due to their low level of sequence homology.

ACKNOWLEDGMENT

We thank Mark Bycroft and Martin Karplus for helpful discussions.

SUPPORTING INFORMATION AVAILABLE

Tables of backbone dynamics data (T_1, T_2, NOE), backbone model-free parameters, side-chain dynamics data (T_1 and $T_{1\rho}$), and side-chain methyl carbon and proton assignments.

REFERENCES

1. Karplus, M., and Petsko, G. A. (1990) *Nature 347*, 631−639.
2. Wand, A. J. (2001) *Nat. Struct. Biol. 8*, 926−931.
3. Palmer, A. G., Rance, M., and Wright, P. E. (1991) *J. Am. Chem. Soc. 113*, 4371−4380.
4. Akke, M., Liu, J., and Palmer, A. G. (1996) *J. Am. Chem. Soc. 118*, 911−912.
5. Muhandiram, D. R., Yamazaki, T., Sykes, B. D., and Kay, L. E. (1995) *J. Am. Chem. Soc. 117*, 11536−11544.
6. Wand, A. J., Urbauer, J. L., McEnvoy, R. P., and Bieber, R. J. (1996) *Biochemistry 35*, 6116−6125.
7. Skrynnikov, N. R., Mulder, F. A. A., Hon, B., Dahlquist, F. W., and Kay, L. E. (2001) *J. Am. Chem. Soc. 123*, 4556−4566.
8. Millet, O., Muhandiram, D. R., Skrynnikov, N. R., and Kay, L. E. (2002) *J. Am. Chem. Soc. 124*, 6439−6448.
9. Chothia, C. (1992) *Nature 357*, 543−544.
10. Orengo, C. A., Jones, D. T., and Thornton, J. M. (1994) *Nature 372*, 631−634.
11. Ponting, C. P., and Russell, R. R. (2002) *Annu. Rev. Biophys. Biomol. Struct. 31*, 45−71.
12. Carr, P. A., Erickson, H. P., and Palmer, A. G. (1997) *Structure 5*, 949−959.
13. Constantine, K. L., Friedrichs, M. S., Wittekind, M., Jamil, H., Chu, C.-H., Parker, R. A., Goldfarb, V., Mueller, L., and Farmer, B. T. (1998) *Biochemistry 37*, 7965−7980.
14. Johansson, M. U., Nilsson, H., Evenäs, J., Forsén, S., Drakenberg, T., Björck, L., and Wikström, M. (2002) *J. Mol. Biol. 316*, 1083−1099.
15. Zhang, F., and Bruschweiler, R. (2002) *J. Am. Chem. Soc. 124*, 12654−12655.
16. Johnson, E. C., and Handel, T. M. (1999) *J. Biomol. NMR 15*, 135−143.
17. Finerty, P. J., Muhandiram, R., and Forman-Kay, J. D. (2002) *J. Mol. Biol. 322*, 605−620.
18. Kay, L. E., Muhandiram, D. R., Farrow, N. A., Aubin, Y., and Forman-Kay, J. D. (1996) *Biochemistry 35*, 361−368.
19. Kay, L. E., Muhandiram, D. R., Wolf, G., Shoelson, S. E., and Forman-Kay, J. D. (1998) *Nat. Struct. Biol. 5*, 156−163.
20. Lee, A. L., Kinnear, S. A., and Wand, A. J. (2000) *Nat. Struct. Biol. 7*, 72−77.
21. Lee, A. L., and Wand, A. J. (2001) *Nature 411*, 501−504.
22. Lee, A. L., Sharp, K. A., Kranz, J. K., Song, X.-J., and Wand, A. J. (2002) *Biochemistry 41*, 13814−13825.
23. Cota, E., Steward, A., Fowler, S. B., and Clarke, J. (2001) *J. Mol. Biol. 305*, 1185−1194.
24. Hamill, S. J., Steward, A., and Clarke, J. (2000) *J. Mol. Biol. 297*, 165−178.
25. Cota, E., Hamill, S. J., Fowler, S. B., and Clarke, J. (2000) *J. Mol. Biol. 302*, 713−725.
26. Ishima, R., Louis, J. M., and Torchia, D. A. (1999) *J. Am. Chem. Soc. 121*, 11589−11590.
27. Lee, A. L., Flynn, P. F., and Wand, A. J. (1999) *J. Am. Chem. Soc. 121*, 2891−2902.
28. Hamill, S. J., Meekhof, A. E., and Clarke, J. (1998) *Biochemistry 37*, 8071−8079.
29. Mardon, H. J., and Grant, K. E. (1994) *FEBS Lett. 340*, 197−201.
30. Miroux, B., and Walker, J. E. (1996) *J. Mol. Biol. 260*, 289−298.
31. Meekhof, A. E., Hamill, S. J., Arcus, V. L., Clarke, J., and Freund, S. M. V. (1998) *J. Mol. Biol. 282*, 181−194.
32. Main, A. L., Harvey, T. S., Baron, M., Boyd, J., and Campbell, I. D. (1992) *Cell 71*, 671−678.
33. Sattler, M., Schleucher, J., and Griesinger, C. (1999) *Prog. Nucl. Magn. Reson. Spectrosc. 34*, 93−158.
34. Neri, D., Szyperski, T., Otting, G., Senn, H., and Wüthrich, K. (1989) *Biochemistry 28*, 7510−7516.
35. Goddard, T. D., and Keller, D. G. (2001) *SPARKY 3*, University of California, San Francisco.
36. Dosset, P., Hus, J.-C., Blackledge, M., and Marion, D. (2000) *J. Biomol. NMR 16*, 23−28.
37. Lipari, G., and Szabo, A. (1982) *J. Am. Chem. Soc. 104*, 4546−4559.
38. Skrynnikov, N. R., Millet, O., and Kay, L. E. (2002) *J. Am. Chem. Soc. 124*, 6449−6460.
39. Mittermaier, A., and Kay, L. E. (1999) *J. Am. Chem. Soc. 121*, 10608−10613.
40. Press, W. H., Teukolsky, S. A., Vetterling, W. T., and Flannery, B. P. (1992) *Numerical recipes in C*, 2nd ed., Cambridge University Press, Cambridge, U.K.
41. Vuister, G. W., Wang, A. C., and Bax, A. (1993) *J. Am. Chem. Soc. 115*, 5334−5335.
42. Bax, A., Max, D., and Zax, D. (1992) *J. Am. Chem. Soc. 114*, 6923−6925.
43. Mittermaier, A., Kay, L. E., and Forman-Kay, J. D. (1999) *J. Biomol. NMR 13*, 181−185.
44. Yang, D., Mok, Y.-K., Forman-Kay, J. D., Farrow, N. A., and Kay, L. E. (1997) *J. Mol. Biol. 272*, 790−804.
45. Liu, W., Flynn, P. F., Fuentes, E. J., Krantz, J. K., McCormick, M., and Wand, A. J. (2001) *Biochemistry 40*, 14744−14753.

46. Leahy, D. J., Hendrickson, W. A., Aukhil, I., and Erickson, H. P. (1992) *Science 258*, 987−991.
47. Leahy, D. J., Aukhil, I., and Erickson, H. P. (1996) *Cell 84*, 155−164.
48. Pontius, J., Richelle, J., and Wodak, S. (1996) *J. Mol. Biol. 264*, 121−136.
49. Dickinson, C. D., Veerapandian, B., Dai, X.-P., Hamlin, R. C., Xuong, N.-H., Ruoslahti, E., and Ely, K. R. (1994) *J. Mol. Biol. 236*, 1079−1092.
50. Halle, B. (2002) *Proc. Natl. Acad. Sci. U.S.A. 99*, 1274−1279.
51. Chou, J. J., Case, D. A., and Bax, A. (2003) *J. Am. Chem. Soc. 125*, 8959−8966.
52. Wong, K.-B., and Daggett, V. (1998) *Biochemistry 37*, 11182−11192.
53. Mittermaier, A., Davidson, A. R., and Kay, L. E. (2003) *J. Am. Chem. Soc. 125*, 9004−9005.
54. Markley, J. L., Bax, A., Arata, Y., Hilbers, C. W., Kaptein, R., Sykes, B. D., Wright, P. E., and Wüthrich, K. (1998) *J. Mol. Biol. 280*, 933−952.
55. Karplus, M., Ichiye, T., and Pettitt, B. M. (1987) *Biophys. J. 52*, 1083−1085.
56. Cota, E., and Clarke, J. (2000) *Protein Sci. 9*, 112−120.
57. Makhatadze, G. I., Loladze, V. V., Ermolenko, D. N., Chen, X. F., and Thomas, S. T. (2003) *J. Mol. Biol. 327*, 1135−1148.
58. Makhatadze, G. I., and Privalov, P. L. (1993) *J. Mol. Biol. 232*, 639−659.
59. Privalov, P. L., and Makhatadze, G. I. (1993) *J. Mol. Biol. 232*, 660−679.
60. Kraulis, P. J. (1991) *J. Appl. Crystallogr. 24*, 946−950.

BI035658E